A Study of the Noise Source Mechanisms in an Excited Mach 0.9 Jet - Complementary Experimental and Computational Analysis

Michael Crawley*, Rachelle L. Speth†, Datta V. Gaitonde‡, and Mo Samimy§
Mechanical and Aerospace Engineering, The Ohio State University, Columbus, OH

The abstract goes here...

I. Introduction

Engine exhaust constitutes one of the major components of aircraft noise during takeoff and landing, and hence poses a significant health concern for community and military personnel. Mitigation of the aeroacoustic noise generated by free jets is therefore a necessity for the both the commercial and military aviation industries. Current noise reduction technologies such as increased bypass ratios or geometric modifications to the nozzle (tabs, chevrons, and lobed mixers), though effective, have associated performance penalties in terms of added weight, drag, or loss of thrust - penalties that are incurred over the entire duration of the flight. A shift to active control technology thus desirable in order to minimize the performance penalties while maximizing the noise reduction, however the proper application of control is not readily apparent. In the simulated two-dimensional shear layer of Wei & Freund[1] a generalized actuator was able to reduce the noise along a prescribed line in the acoustic field by up to 11 dB. The researchers observed that the excitation was not altering the broad characteristics of the shear layer (such as turbulent kinetic energy) or even the evolution of the most energetic structures in an appreciable manner. Rather, the control appeared to be effecting the acoustic field by regularizing the large-scale structures, thereby reducing the radiating efficiency of the noise sources. Clearly, fundamental understanding of the noise sources and radiating mechanisms is required for efficient and effective active noise mitigation strategies.

Perhaps the most well-known source model for jet mixing noise is the two-component model of Tam *et al.*,[2] which recognized that the acoustic far-field spectra of jets can be represented as two distinct universal similarity spectra, irrespective of jet Mach number or temperature ratio. In this model, the incoherent fine-scale mixing layer turbulence, produces an incoherent, broadband acoustic field and is believed to be the dominant source of acoustic radiation at sideline angles. In contrast, aft angle radiation is dominated by the large-scale structures and exhibit a strong spectral peak. Theoretical analysis by Tam[3] demonstrated Mach wave radiation emitted through the supersonic convective of these large scale structures - the oft-mentioned "wavy-wall" analogy. This analysis was extended in Tam & Burton[4] to include amplification and decay of the structures, through which subsonically-convecting structures were found to emit noise (this structure evolution was also shown to broaden the directivity and frequency bands of the acoustic radiation). Experiments utilizing direct correlations between density and velocity fluctuations in the shear layers of high-speed jets and the acoustic far-field have supported this two-component source model.[5,6]

That the large-scale structures are the dominant noise sources in the turbulent jet is beyond doubt at this point. Yet, the exact dynamics that govern the evolution of the structures and ultimately the noise emission are still not fully understood. The intermittent nature of the structures and noise emission was first observed by Hileman *et al.*[7] in a supersonic jet. Simplified source models utilizing temporally and spatially modulated wavepackets were found to reproduce the superdirective character observed in the far-field spectra, as well

*Graduate Research Assistant. Student Member, AIAA
†Graduate Research Assistant. Student Member, AIAA
‡John Glenn Chair Professor. Fellow, AIAA
§John B. Nordholt Professor. Fellow, AIAA

as improve the match between the observed and predicted spectral amplitudes.[8–10] Hence, understanding the exact spatiotemporal evolution of the large-scale structures is important to predicting and ultimately controlling their radiation production.

II. Experimental Setup

Experimentation was conducted in the free jet facility (a schematic of which can be found in Fig. 1) at the GDTL within the Ohio State University's Aerospace Research Center.The dimensions of the chamber are 5.14 m wide by 4.48 m long and 2.53 m high (wedge-tip to wedge-tip). The design of the chamber produces an anechoic cutoff frequency of 160 Hz, below the frequencies of interest for this study. Additional details of the facility design and validation can be found in Hahn.[11] Compressed, dried, and filtered air is supplied by two cylindrical storage tanks with a total capacity of 43 m^3 and maximum pressure of 16 MPa; the tanks are charged by three, five-stage reciprocating compressors. The air enters the facility horizontally, passes through a stagnation chamber and turbulence screens, and exhausts through a converging nozzle. Opposite the nozzle, a collector accumulates the jet and entrained air and exhausts to the outdoors.

A converging, axisymmetric nozzle with exit diameter of 25.4 mm was used in the current study. The internal contour of the nozzle was designed using a fifth order polynomial. The nozzle utilized a thick-lipped design in order to simplify the mounts for the LAFPA extension, which housed the eight actuators used in this study.For the experiments reported in this paper, the jet was operated at a Mach number, M_j, of 0.90, and with a total temperature ratio of unity.The Reynolds number based on the jet exit diameter was 6.2×10^5; previous investigations using hot-wire anemometry have indicated that the initial shear layer is turbulent for this operating condition with momentum thickness 0.09 mm and boundary layer thickness 1 mm.[12]

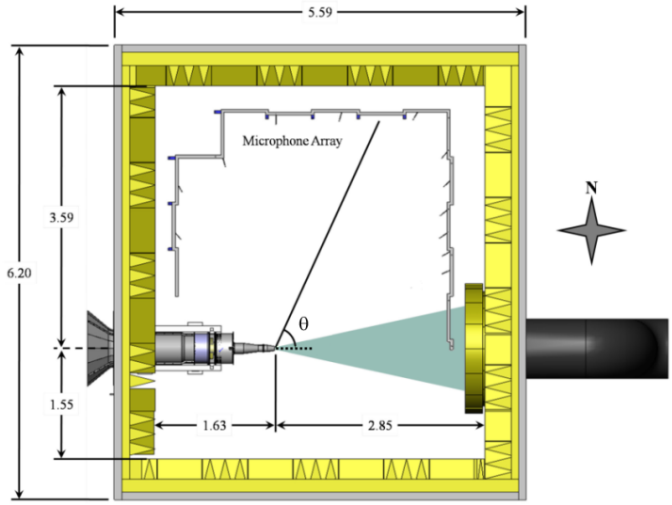

Figure 1: Plan view of GDTL free jet facility; dimensions in meters.

Excitation was applied to jet shear layer via eight LAFPAs which were uniformly spaced around the nozzle perimeter 1 mm upstream of the nozzle exit. Each LAFPA consists of a pair of tungsten pin electrodes with tip spacing (center-to-center) of 4 mm. The electrodes are housed in a boron nitride extension attached to the end of the nozzle.A more detailed description of LAFPA characteristics can be found in Utkin et al.[13] The LAFPAs are energized by a multi-channel, high-voltage plasma power generator capable of simultaneously powering up to eight LAFPAs, which was designed and built in-house at the GDTL. In the second-generation power supply, each individual circuit consists of a switchable capacitor in line with a high voltage transformer; the arcing electrodes are connected to the secondary side of the coil.The switches are controlled by a 16-channel digital I/O card and National Instruments' Labview software, operated by a dedicated computer. The plasma generator provides independent control of the frequency, duty cycle/pulse width, and phase of each individual actuator (though at a constant amplitude of 5 kV).The pulse width was held constant at 7 μs,

which was found to be the minimum pulse width at which the actuators consistently arced for all frequencies explored in this study.[14] In order to improve our understanding of the linear and nonlinear dynamics of the large-scale structure interactions, the excitation Strouhal numbers ranges from 0.02 to 0.50; an azimuthal mode of $m = 0$ was used in all cases.

Near-field and far-field pressure measurements were acquired simultaneously, using Brüel & Kjær 1/4 inch 4939 microphones. The signal from each microphone is band-pass filtered from 20 Hz to 100 kHz using a Brüel & Kjær Nexus 2690 conditioning amplifier, and recorded using National Instruments PXI-6133 A/D boards and LabView software. The microphones are calibrated using a Brüel & Kjær 114 dB, 1 kHz sine wave generator. The frequency response of the microphones is flat up to roughly 80 kHz, with the protective grid covers removed. Voltage signals are collected at 200 kHz with 81920 data points per block; sub-blocks of 8192 data points were used when calculating short-time power spectral densities, resulting in a frequency resolution of 24.4 Hz. Ten blocks were recorded for each case, resulting in four seconds of data. Analysis of the far-field acoustic spectra found this length to be sufficient for statistical convergence of the turbulence statistics.

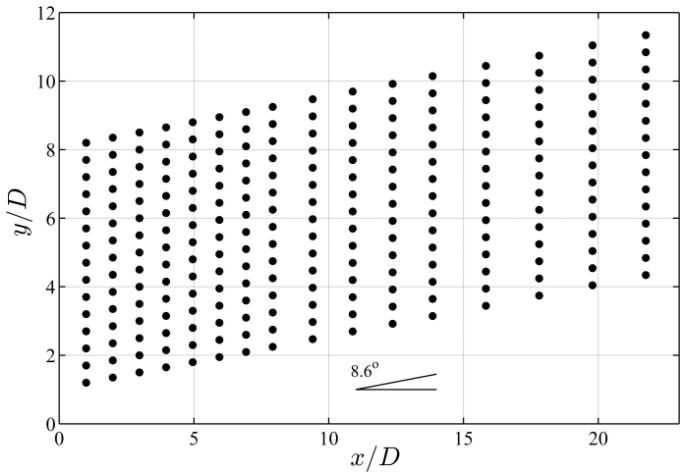

Figure 2: Near-field microphone array grid.

Far-field acoustic pressure is acquired at three polar angles: 30°, 60° and 90°, as measured from the downstream jet axis. The radial distance of the microphones ranges from 101D at 30° to 145D at 60°. The near-field pressure was acquired using a linear array of sixteen microphones located along the meridional plane of the jet; the spacing varied along the array from 1D to 2D (Fig. 2). The linear array is mounted to a traverse system at an angle of 8.6° to the jet axis in order to match the spreading angle of the jet shear layer for this Mach number.[12] The traverse is controlled using LabView and enables the acquisition of pressure measurements at various radial positions with respect to the jet axis. Initially, the most upstream microphone is positioned at x/D = 1 and r/D = 1.20, to ensure that the microphone tips are outside the mixing layer and do not affect the flow field. For subsequent cases, the microphone array is incremented radially outward by 0.5D for a total travel distance of 7D. Signals from the near-field array are preprocessed in order to remove actuator-self noise while retaining the true hydrodynamic and acoustic response of the jet. This has been accomplished via a filter operating in the continuous wavelet domain. Further details may be found in Crawley et al.[15]

III. Computational Model

The simulations employ the same approach as previously used to simulate a Mach 1.3 jet without and with control.[16,17] The full compressible Navier-Stokes equations are solved in curvilinear coordinates (ξ, η, ζ) using the strong conservative form.[18,19] The transformed non-dimensional equations in vector notation are given as:

$$\frac{\partial}{\partial \tau}\left(\frac{\vec{U}}{J}\right) + \frac{\partial \hat{F}}{\partial \xi} + \frac{\partial \hat{G}}{\partial \eta} + \frac{\partial \hat{H}}{\partial \zeta} = \frac{1}{Re}\left[\frac{\partial \hat{F}_v}{\partial \xi} + \frac{\partial \hat{G}_v}{\partial \eta} + \frac{\partial \hat{H}_v}{\partial \zeta}\right] \tag{1}$$

where $\vec{U} = \{\rho, \rho u, \rho v, \rho w, \rho E\}$ denotes the solution vector and $J = \partial(\xi, \eta, \zeta, \tau)/\partial(x, y, z, t)$ is the transformation Jacobian. Details of the various terms in Eqn. 1 may be found in Speth and Gaitonde.[20] For the inviscid terms, a third-order upwind biased approach is adopted, together with the Roe scheme[21] for flux evaluation. The limiter required to enforce monotonicity is a crucial component of the method. The van Leer harmonic limiter[22] has proven to be very successful at reproducing the main features of the unsteadiness in the jet. The viscous terms are discretized with second-order centered differences and time integration is performed by a second-order diagonalized[23] approximately factored method.[24] A sub-iteration strategy is used to minimize errors due to factorization, linearization and explicit boundary condition implementation.

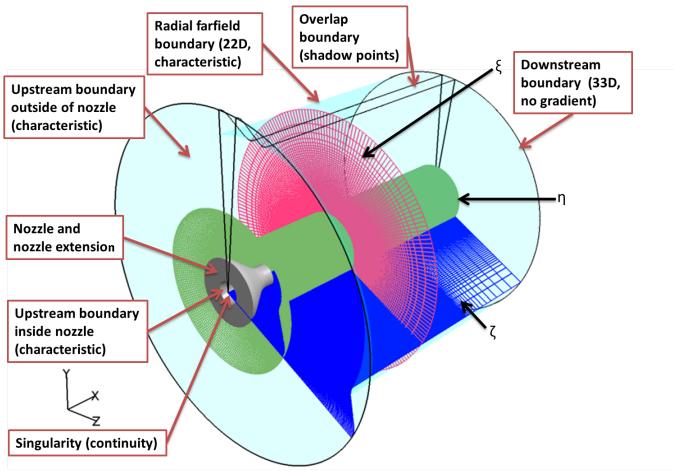

Figure 3: Computational domain

A 65 million point mesh (Fig. 3) is used to simulate the Mach 0.9 jet measured in the experiment (Fig. **??**a). The grid has dimensions of 685 points on the ξ (streamwise) direction, 455 points in the η (radial) direction, and 209 points in the ζ (azimuthal) direction. In the radial direction, the mesh is refined in the nozzle region and gradually stretched in the far field. At the exit of the nozzle, the grid maintains a constant axial spacing until after the potential core length; then stretches in the streamwise direction as well. To preserve continuity, the grid has a five point overlap in the ζ direction. Characteristic boundary conditions[25] are applied to the upstream (outside the nozzle) and radial boundaries. Non-reflecting conditions are applied to the downstream and far-field boundaries. Stagnation conditions are specified at the first ξ plane of the nozzle ($\rho_{inlet} = 2.04 kg/m^3$, $U_{inlet} = 22 m/s$, $P_{inlet} = 171,427 Pa$) to achieve perfectly expanded nozzle exit conditions corresponding to $\rho_{jet} = 1.404 kg/m^3$, $U_{jet} = 285.99 m/s$, $T_{jet} = 251.31 K$ which match the experiments. Based on the nozzle diameter therefore, the Reynolds number is $Re = 635,308$. The nozzle geometry resembles that of the experiments including the nozzle ring on which the actuators are mounted. The velocity profile at the entrance to the nozzle is that of a uniform flow (zero at the wall and U_{inlet} everywhere else). Perturbations were not introduced into the inflow due to the unknown perturbations in the experiment. Therefore, the simulations have a laminar boundary layer at the nozzle exit while the experiments have a very thin turbulent boundary layer (the momentum thickness has been estimated to be $0.09mm$). Previous studies have shown that despite this difference, the main features of the experimental observations are successfully reproduced by the computations.[16,17] Other studies have shown that a smaller 32 million point simulation is adequate to reproduce the features of the experiment.[26]

The LAFPAs are modeled after the experiments using a surface heating technique to excite jet shear layer instabilities and azimuthal modes within the jet. Eight actuators are placed around the periphery of the jet on the nozzle collar at the locations and dimensions of the experiments as explained previously. As shown in Fig. 4b, each actuator consists of a heated region of the nozzle wall which extends the azimuthal length corresponding to the separation distance between electrodes ($3mm$) and has an axial extent equal to the length of the groove ($1mm$). The temperature of the nozzle wall was assumed to be $1.12T_\infty$. When the actuator is on the temperature of the actuator region increases to $5T_\infty$. Little difference was seen in the previous work (Speth and Gaitonde[27]) for the temperature range measured in experiments (Utkin *et al.*[28]) for a Mach number of 1.3. The semi-empirical model is necessary to avoid first-principles simulation of the poorly understood plasma heating process, as well as to restrict the required computational resources to

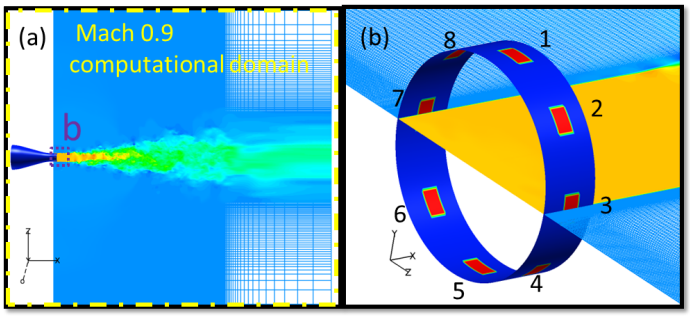

Figure 4: The computational domain including the nozzle (a), and the numerical actuator model (b)

feasible levels (see Ref.[29]).

Unlike acoustic drivers, the LAFPAs are on-off devices and thus can be represented by rectangular pulses with a duty cycle, which allows for a wide range of operation choices. Duty cycle is the percentage of actuator on time in an excitation cycle. Therefore, a duty cycle of 100% results in the actuator being on all the time. The experimental duty cycle varies with frequency, since the arc strike lasts a fixed time. Since the actuator model is empirical, the computational duty cycle was chosen to obtain similar control authority as in the experiment. This necessitates a higher duty cycle (10%) than the one used in the experiments (2.0% for $St_{DF} = 0.25$). As noted earlier, despite the simplicity of the model, its success has been documented in Gaitonde and Samimy,[16] where, in addition to coherent structures, mean and fluctuating quantities have been compared. Furthermore, the mean flow structure with control was shown to match the theoretical predictions of Cohen and Wygnanski.[30]

Like the experiments, the axisymmetric ($m = 0$) mode was employed to study a range of Strouhal numbers. The Strouhal numbers studied in the simulations include: 0.05, 0.15, and 0.25. Data was acquired every timestep at the point probes depicted in Fig. 2 as well as on several ξ, η, and ζ computational planes. Phase-averaged data were also computed for each of the simulations.

IV. Results

V. Conclusions and Future Work

Acknowledgments

Computational resources were provided by the DoD HPCMP (AFRL, NAVO and ERDC) and the Ohio Supercomputer Center. The support of this complementary experimental and computational work by the Air Force Office of Scientific Research (Dr. John Schmisseur and Dr. Rengasamy Ponnappan) is greatly appreciated. Several figures were made using Fieldview software with licenses obtained from the Intelligent Light University Partnership Program.

References

[1]Wei, M. and Freund, J. B., "A noise-controlled free shear flow," *Journal of Fluid Mechanics*, Vol. 546, 2006, pp. pp. 123–152.

[2]Tam, C. K. W., Golebiowski, M., and Seiner, J. M., "On the Two Components of Turbulent Mixing Noise from Supersonic Jets," *AIAA/CEAS 2nd Aeroacoustics Conference*, Vol. AIAA Paper, State College, PA, May 6-8, 1996.

[3]Tam, C. K. W., "Directional acoustic radiation from a supersonic jet generated by shear layer instability," *Journal of Fluid Mechanics*, Vol. 46, No. 4, 1971, pp. pp. 757–768.

[4]Tam, C. K. W. and Burton, D. E., "Sound generated by instability waves of supersonic flows. Part 2. Axisymmetric jets," *Journal of Fluid Mechanics*, Vol. 138, 1984, pp. pp. 273–295.

[5]Panda, J. and Seasholtz, R. G., "Experimental investigation of density fluctuations in high-speed jets and correlation with generated noise," *Journal of Fluid Mechanics*, Vol. 450, 2002, pp. 97–130.

[6]Panda, J., Seasholtz, R. G., and Elam, K. A., "Investigation of noise sources in high-speed jets via correlation measurements," *Journal of Fluid Mechanics*, Vol. 537, 2005, pp. 349–385.

[7]Hileman, J., Carabalo, E., Thurow, B., and Samimy, M., "Large-Scale Structure Evolution and Sound Emission in High-Speed Jets: Real-Time Visualization with Simultaneous Acoustic Measurements," *J. Fluid Mech.*, Vol. 544, 2005, pp. 277–307.

[8]Sandham, N. D., Morfey, C. L., and Hu, Z. W., "Nonlinear mechanisms of sound generation in a perturbed parallel jet flow," *Journal of Fluid Mechanics*, Vol. 565, 2006, pp. 1–23.

[9]Cavalieri, A. V. G., Jordan, P., Gervais, Y., Wei, M., and Freund, J. B., "Intermittent sound generation and its control in a free-shear flow," *Physics of Fluids*, Vol. 22, No. 11, 2010, pp. 115113–.

[10]Crighton, D. G. and Huerre, P., "Shear-layer pressure fluctuations and superdirective acoustic sources," *Journal of Fluid Mechanics*, Vol. 220, 1990, pp. 355–368.

[11]Hahn, C., *Design and Validation of the New Jet Facility and Anechoic Chamber*, Ph.D. thesis, The Ohio State University, Columbus, OH, 2011.

[12]Kearney-Fischer, M., Kim, J.-H., and Samimy, M., "Control of a High Reynolds Number Mach 0.9 Heated Jet Using Plasma Actuators," *Physics of Fluids*, Vol. 21, No. 9, 2009.

[13]Utkin, Y., Keshav, S., Kim, J.-H., Kastner, J., Adamovich, I., and Samimy, M., "Characterization of Localized Arc Filament Plasma Actuators Used for High-speed Flow Control," *AIAA Paper 2007-0787*, 2007.

[14]Hahn, C., Kearney-Fischer, M., and Samimy, M., "On factors influencing arc filament plasma actuator performance in control of high speed jets," *Experiments in Fluids*, Vol. 51, No. 6, 2011, pp. 1591–1603.

[15]Crawley, M., Sinha, A., and Samimy, M., "Near-field and Acoustic Far-field Response of a High-Speed Jet Forced with Plasma Actuators," *AIAA Journal*, Expected 2015.

[16]Gaitonde, D. and Samimy, M., "Coherent structures in plasma-actuator controlled supersonic jets: Axisymmetric and mixed azimuthal modes," *Phys. Fluids*, Vol. 23, No. 9, 2011.

[17]Speth, R. and Gaitonde, D., "Parametric Study of a Mach 1.3 Cold Jet Excited by the Flapping Mode Using Plasma Actuators," *Computers & Fluids*, 2013.

[18]Vinokur, M., "Conservation Equations of Gasdynamics in Curvilinear Coordinate Systems," *J. Comp. Phys.*, Vol. 14, 1974, pp. 105–125.

[19]Steger, J., "Implicit Finite-Difference Simulation of Flow about Arbitrary Two-Dimensional Geometries," *AIAA Journal*, Vol. 16, No. 7, July 1978, pp. 679–686.

[20]Speth, R. and Gaitonde, D., "The Effect of Laminar Nozzle Exit Boundary Layer Thickness on a Mach 1.3 Jet With and Without Control," *42nd AIAA Fluid Dynamics Conference and Exhibit*, 2012.

[21]Roe, P., "Approximate Riemann Solvers, Parameter Vectors and Difference Schemes," *Journal of Computational Physics*, Vol. 43, 1981, pp. 357–372.

[22]van Leer, B., "Towards the Ultimate Conservation Difference Scheme V, A Second-Order Sequel to Godunov's Method," *Journal of Computational Physics*, Vol. 32, 1979, pp. 101–136.

[23]Pulliam, T. and Chaussee, D., "A Diagonal Form of an Implicit Approximate-Factorization Algorithm," *J. Comp. Phys.*, Vol. 39, No. 2, 1981, pp. 347–363.

[24]Beam, R. and Warming, R., "An Implicit Factored Scheme for the Compressible Navier-Stokes Equations," *AIAA Journal*, Vol. 16, No. 4, 1978, pp. 393–402.

[25]Bellan, J., "Supercritical (and Subcritical) Fluid Behavior and Modeling: Drops, Streams, Shear and Mixing Layers, Jets and Sprays," *Prog. Energy Combust. Sci.*, Vol. 26, 2000, pp. 329–366.

[26]Speth, R. and Gaitonde, D., "Correlation of Near Field Pressure with Coherent Structures in an Excited Mach 1.3 Jet," *ASME 2013 Fluids Engineering Division Summer Meeting*, No. FEDSM2013-16495, 2013.

[27]Speth, R. and Gaitonde, D., "Parametric Study of a Supersonic Jet Subjected to Plasma-based Flapping Mode Excitation," *AIAA Paper 2012-0901*, 2012.

[28]Utkin, Y., Keshav, S., Kim, J.-H., Kastner, J., Adamovich, I., and Samimy, M., "Use of Localized Arc Filament Plasma Actuators for High Speed Jet Control," *J. Phys. D: Applied Physics*, Vol. 40, Feb 2007, pp. 685–694.

[29]Gaitonde, D., "Analysis of plasma-based flow control mechanisms through large-eddy simulations," *Computers and Fluids*, Vol. 85, 2013, pp. 19–26.

[30]Cohen, J. and Wygnanski, I., "The evolution of instabilities in the axisymmetric jet. Part 2. The flow resulting from the interaction between two waves," *J. Fluid Mech.*, Vol. 176, 1987, pp. 221–235.